29th AIAA Applied Aerodynamics Conference
27 - 30 June 2011, Honolulu, Hawaii

AIAA 2011-3176

A Systematic Study on the Impact of Dimensionality for a Two-Dimensional Aerodynamic Optimization Model Problem

John C. Vassberg*, Neal A. Harrison†, Dino L. Roman‡
Boeing Research & Technology, The Boeing Company, Huntington Beach, CA 92647

Antony Jameson§
Department of Aeronautics and Astronautics, Stanford University, Stanford, CA 94305

Abstract

A model problem, based on the NACA0012 airfoil, is studied. The thickness distribution of the symmetric NACA0012 airfoil is optimally approximated with a 4^{th}-order Bezier curve. This best-fit approximation is designated Bez4-0012. Introducing this approximation is similar to the first step taken in optimization methods which work on an absolute analytic definition of an existing geometry, rather than on a perturbation of the baseline shape. Advantages and disadvantages of these approaches are discussed. In order to systematically study the impact of dimensionality, an infinite family of design spaces is developed. This family has the property that all airfoil shapes supported in its M-space are fully and exactly contained within its N-space, where $3 \leq M \leq N$. Response-surface and gradient-based methods of optimization are applied. Results for design-space dimensions of $[3, 6, 12, 24, 36]$ are presented. These data include trends with respect to increasing dimension on realized minimum-drag designs, and computational costs.

Nomenclature

CFD	**Computational Fluid Dynamics**
C_d	**Drag Coefficient** $= \frac{drag}{q_\infty C_{ref}}$
C_P	**Pressure Coefficient** $= \frac{P-P_\infty}{q_\infty}$
C_{ref}	**Airfoil Reference Chord** $= 1.0$
$count$	**Drag Coefficient Unit** $= 0.0001$
LE	**Airfoil Leading Edge**
M	**Mach Number** $= \frac{V}{a}$
q	**Dynamic Pressure** $= \frac{1}{2}\rho V^2$
$RANS$	**Reynolds-Averaged Navier-Stokes**
t	**Thickness of an Airfoil**
TE	**Airfoil Trailing Edge**
x	**Streamwise Cartesian Coordinate**
y	**Vertical Physical Coordinate**
$2D$	**Two Dimensional**
α	**Angle-of-Attack**
τ	**TE Included Angle**
ρ	**Radius of Curvature**
∞	**Signifies Freestream Conditions**

*Boeing Technical Fellow, Fellow AIAA
†Engineer, AIAA Senior Member
‡Boeing Associate Technical Fellow, AIAA Associate Fellow
§Thomas V. Jones Professor of Engineering, Fellow AIAA

I. Introduction

Over the past four decades computational fluid dynamics (CFD) has matured to the level that very accurate aerodynamic performance analyses are now possible for complete aircraft configurations, provided that the flow of the viscous shear layers remain predominately attached to the geometry surfaces. Fortunately, this is usually the case for well-designed aircraft at their intended cruise flight conditions.

Concurrent with the advancement of CFD, aerodynamic shape optimization, and multi-disciplinary optimization have also matured to the stage that they have been successfully incorporated into the aircraft design environment, and now perform crucial roles. However, the costs associated with these optimizations can be quite large, and even prohibitive, for many problems of practical interest. These costs include both computational resources as well as engineering labor hours needed to set up the problems for optimization. Even though advancements in computer hardware continue to track Moore's Law, so do the size of our CFD models for analysis. As a consequence, research directed towards improving the efficiencies of optimizations continue.

The work presented herein addresses the impact of the dimensionality of the design space on a simple model problem. An aerodynamic shape optimization of a two-dimensional (2D) non-lifting inviscid symmetric airfoil is studied. This model problem is chosen such that characteristics of reasonably-large design-space dimensions can be considered without incurring a detrimental computational expense.

This paper is organized in the following manner. Section II provides a description of the baseline airfoil geometry and its development. Section III describes the infinite family of design spaces adopted for this study. Section IV illustrates the 2D grid system and discusses measures taken to maintain consistancy in the field grids across airfoil shape changes. Section V develops the model problem studied in the present work. Section VI describes the CFD methods utilized. Section VII describes the optimization techniques employed. Section VIII provides the results of the study. Section IX summarizes our conclusions. Section X discusses how this work spawned another study. Tables of data are embedded within the text, while all figures are appended to the end of the paper.

II. Bez4-0012 Baseline Geometry

This section provides a description of the baseline airfoil utilized in this study. This geometry is based on the symmetric NACA0012 airfoil section, however with the closed trailing-edge modification of Vassberg.[1]

Abbott and von Doenhoff[2] give the analytic equation defining the NACA0012 airfoil as:

$$y_N(x) = \pm\frac{0.12}{0.2}\left(0.2969\sqrt{x} - 0.1260x - 0.3516x^2 + 0.2843x^3 - 0.1015x^4\right). \tag{1}$$

The numerator of the lead terms in Eqn (1) (i.e., 0.12) is the "thickness" of the airfoil. The standard NACA0012 airfoil is defined over the interval: $0 \le x \le 1$. However, at $x = 1$, the y coordinate does not vanish, and therefore, the trailing edge is not sharp, but rather has about a 0.42%-thick blunt base.

In order to avoid issues related to the solution of inviscid flows about aft-facing steps, the airfoil chord is extended so that the trailing-edge point coincides with the neighboring root of Eqn (1). (Although the actual chord length of this airfoil is slightly greater than one, a reference chord of one is adopted.) The resulting sharp trailing-edge location is:

$$x_{TE} = 1.0089304115. \tag{2}$$

In the present work, the thickness distribution of the NACA0012 airfoil, given by Eqn (1) over the interval $0 \le x \le x_{TE}$, is optimally approximated by a 4^{th}-order Bezier curve as follows.

Consider a 2D Bezier curve parameterized by $0 \le u \le 1$, where $u = 0$ represents the airfoil leading edge (LE), and $u = 1$ its trailing edge (TE). Also constrain the slope of this curve to be vertical at the LE, hence $\frac{dx}{du} = 0$ and $\frac{dy}{du} \neq 0$ at $u = 0$. A 4^{th}-order Bezier curve conforming to these conditions has knot coordinates:

$$\begin{aligned} xk_0 &= 0, \quad xk_1 = 0, \quad xk_4 = 1.0089304115, \\ yk_0 &= 0, \quad yk_1 \neq 0, \quad yk_4 = 0. \end{aligned} \tag{3}$$

This leaves 5 free variables in knot coordinates that can be manipulated to define a best-fit curve. Now let I be a cost function that provides a measure of the geometric difference between the Bezier curve and the NACA0012 airfoil, defined as:

$$I = \int_0^1 [y_B(u) - y_N(x(u))]^2 \, du. \tag{4}$$

Here, y_B and y_N are the Bezier and NACA0012 equations, respectively. A minimization of this cost function yields a best-fit 4^{th}-order Bezier curve, which we have designated Bez4-0012. The knots of Bez4-0012 are provided in Table I. Figure 1 illustrates the Bez4-0012 airfoil shape, and its corresponding knots and hull. Note that the y-coordinate is amplified for clarity.

Table I: Bez4-0012 Knots.

n	xk_n	yk_n
0	0.0000000	0.0000000
1	0.0000000	0.0256211
2	0.0525433	0.0443137
3	0.1821054	0.1119573
4	1.0089304	0.0000000

The knots of Table I minimize the cost function of Eqn 4 as:

$$I_{min} \doteq 0.8149 * 10^{-8}. \tag{5}$$

Figure 2 depicts the shape difference between the Bez4-0012 and NACA0012 airfoil sections. In this figure, $YDIFF = [y_B - y_N]$. A comparison of several geometric quantities for the Bez4-0012 and NACA0012 airfoils are tabulated in Table II. Note that the LE radius of the Bez4-0012 airfoil is slightly larger than that of the NACA0012. Whereas the TE included angle, τ, and the maximum thickness of Bez4-0012 are slightly reduced from those of NACA0012.

Table II: Bez4-0012 vs. NACA0012.

Metric	Bez4-0012	NACA0012
ρ_{LE}	0.01666	0.01587
τ_{TE}	15.4226°	16.1501°
x_{tmax}	0.29844	0.29983
t_{max}	0.11987	0.12003

The next section describes the infinite family of design spaces utilized in this work.

III. Design Space

In the present study, an infinite family of design spaces is constructed which has the property that all possible airfoil shapes supported by its M-space are fully contained in its N-space, where $3 \leq M \leq N$. Recall the Bez4-0012 airfoil with knots given in Table I. For the aerodynamic shape optimizations performed in this study, only the internal y-knots ($yk_n, 1 \leq n \leq N$) are used as design variables. Here, N is the dimension of the design space, and $K = N + 1$ is the order of the Bezier curve associated with the N-space. For example, a 4^{th}-order Bezier curve is defined by 5 knots ($0 \leq k \leq K = 4$). Since only the internal y-knots (yk_n; $1 \leq n \leq N = 3$) are used as design variables, an arbitrary 4^{th}-order Bezier curve pinned at the LE and TE end-points with fixed x-knot locations given by Table I defines our 3-space.

In order to satisfy the property that any M-space is a subset of any N-space, where $3 \leq M \leq N$, we utilize a recursive degree elevation of the Bez4-0012 baseline airfoil. This process is illustrated in Figure 3, where the knots of Bez4-0012 are elevated from its native 3-space to an equivalent airfoil in 4-space. In general,

elevating a K^{th}-order Bezier curve to $(K+1)^{st}$ order has knots given by the following recursive formula.

$$B_k^{(K+1)} = \left(\frac{k}{K+1}\right) B_{k-1}^{(K)} + \left(\frac{K+1-k}{K+1}\right) B_k^{(K)}; \;\; where\; 0 \le k \le K+1. \tag{6}$$

Here, $B^{(K)}$ and $B^{(K+1)}$ represent the knots of the K^{th}-order and $(K+1)^{st}$-order Bezier curves, respectively. Note that while $B_{-1}^{(K)}$ and $B_{K+1}^{(K)}$ do not exist, their weighting factors in Eqn (6) are zero.

To complete the discussion on the design space, we introduce a straightforward constraint on the allowable space for design. In this study, the thickness of the optiumum airfoil must be greater than or equal to that of the baseline Bez4-0012. Hence, the following condition must hold for the optimum shape.

$$y_{Bez4-0012} \le y_{Optimum} \;;\;\; 0 \le u \le 1. \tag{7}$$

Note that this constraint is only imposed on the final optimum geometry. Shapes that violate this condition are allowed during the optimization process.

Grid generation used in the present work is discussed in the next section.

IV. Grid Generation

The two-dimensional grids utilized in this study are based on the (256x256) O-mesh of Vassberg and Jameson.[1] This grid was developed about the closed-TE NACA0012 airfoil. A close-up view of this mesh is shown in Figure 4. Note the high-quality of this nearly-conformal grid. The farfield resides about 150 chord lengths away from the airfoil geometry.

In the present work, a similar grid is constructed for each airfoil shape studied by applying the following mesh perturbation to the grid of Figure 4.

$$ym_{Bi,j} = ym_{Ni,j} + \left[\frac{e^{2\pi} - e^{2\pi(\frac{j-1}{NC})}}{e^{2\pi}-1}\right] * \left[y_{Bi} - y_{Ni}\right] \quad ; \quad 1 \le i,j \le NC+1. \tag{8}$$

Here, $ym_{Bi,j}$ is the y-coordinate of mesh point (i,j) for the new mesh conforming to y_B. $ym_{Ni,j}$ is the y-coordinate of the NACA0012 mesh of Vassberg and Jameson.[1] y_B is the y-coordinate of the Bezier airfoil, and y_N corresponds to the NACA0012 section. Subscript i is a grid index that wraps around the airfoil in a clockwise direction, starting at the TE. Subscript j is 1 at the airfoil surface and at its maximum value at the farfield boundary. In addition to this, the resulting grid is forced to be exactly symmetric about the x-axis. This mesh deformation procedure is utilized herein to maintain as close as possible a self-similar family of grids throughout the optimization process.

The next section describes the model problem investigated herein.

V. Model Problem

The model problem under study is to mimimize the drag of a symmetric airfoil, subject to the geometric constraint given by Eqn (7), for the inviscid transonic flow condition of $M = 0.85$, and $\alpha = 0^\circ$. The flow physics of this model problem is such that the only source for drag is that associated with any shocks that may arise. The problem was crafted with an anticipation that a shock-free design is impossible.

This two-dimensional inviscid compressible flow problem is chosen to provide a nonlinear objective function, yet one that only requires moderate computational costs to evaluate. With the inexpensive nature of computing the objective function, it is feasible to survey a wide range of design-space dimensions. The product of this study is to develop a better understanding of the characteristics of various optimization processes; the resulting optimum airfoils are of little consequence.

The next section describes the computational fluid dynamic methods utilized herein.

VI. CFD Methods

In the present study, two CFD methods are utilized, namely OVERFLOW and FLO82. The only flow condition under study is the transonic condition of $M = 0.85$, and $\alpha = 0^\circ$ angle-of-attack. Since the airfoils

herein are symmetric, the resulting lifting condition is $C_l = 0.0$ (bold assumption). This removes any requirement for a point-vortex influence on the farfield boundary conditions.

OVERFLOW[3] is a general-purpose CFD method developed by NASA in the early 1990s. OVERFLOW is capable of solving either the three-dimensional Euler or RANS equations using multiple overset structured grids. It can be applied to very complex geometries. In this investigation, OVERFLOW is used to solve the two-dimensional inviscid compressible flow about symmetric non-lifting airfoil sections. The version of OVERFLOW studied is (2.1t). Unless otherwise noted, all OVERFLOW solutions are performed on a high-quality single-block (256x256) O-mesh as described in the previous section.

FLO82[4] is a cell-centered Euler method based on an O-mesh. Upwinding is provided by the H-CUSP dissipation scheme of Jameson.[5] In general, FLO82 includes the influence of a point-vortex on the farfield boundary condition for lifting conditions.

The next section describes the optimization methods utilized in our work.

VII. Optimization Methods

In the present work, two different approaches are applied to perform the aerodynamic shape optimization for the model problem under study. These methods are described next.

MDOPT[6] is a Boeing multidisciplinary design optimization framework for very general air vehicle design and analysis. The system contains a collection of technology modules for performing optimization studies by means of a Graphical User Interface (GUI), and combining robust numerical optimization schemes with higher-order computational analysis. A variety of multidisciplinary objective and constraint functions are available, including aerodynamic, weight, mission performance, and stability and control characteristics. MDOPTs GUI environment helps manage the tasks of: 1) design-space set-up, 2) establishing a design of experiments, 3) fitting the response surface, 4) navigating the response surface to the optimum state, 5) perturbing field grid points, and 6) enforcing a variety of nonlinear constraints. MDOPT can be exercised in two modes, the first being based on response surfaces, and the second being a direct-driven quasi-Newton method. In the current work, only the response-surface approach is studied.

SYN83[7] utilizes an adjoint to the Euler equations to compute the gradient of the design space with respect to the objective function. Here, the design space is automatically generated by SYN83; it corresponds to the highest dimensional space supported by the discrete points of the grid defining the geometry. Hence, the performance of the resulting optimum airfoil could provide a limit to what is achievable, unless the optimization locates a local optimum that is quite degraded from the globally best design. SYN83 solves both the Euler equations and its adjoint on an internally-generated C-mesh. The optimization process begins by solving converged solutions on both the Euler equations and its adjoint for the baseline airfoil shape. Then its design space is navigated in the reverse direction of the gradient projected into a Sobolev space. This continues until the magnitude of the gradient vanishes. Upon completion of the run, a locally-optimum airfoil is found and a converged solution of the Euler equations on this shape is known. In practice, the complete SYN83 optimization process is only about one-order-of-magnitude greater than the cost of a single analysis. SYN83 is used herein to establish an optimimum goal objective level. This goal was purposely not established until *after* the first phase of the MDOPT investigations had been completed.

The next section provides the final results of this study.

VIII. Results

This section presents the results of this study, organized into three chronological phases. The first phase is a discovery exercise for the first three authors to become familiar with appying MDOPT to this model problem. Although the model problem was specifically designed to be computationally inexpensive per case analyzed, it was also crafted to be a very nonlinear problem of optimization, as well as to be an unfamiliar case to investigate. The purpose for choosing an unfamiliar case was to measure our level of success under a blind test. Initially, no preconceived notion of what level of improvement could be attained was available. This phase required many optimizations and re-optimizations to improve our level of expertise, as well as to obtain self-consistant results across the design spaces studied. We note that our unfamiliarity was with the model problem, not with the application of MDOPT.

The second phase introduced a SYN83 optimization to provide an optimum airfoil from a very-high-dimension design space. This effort was performed independently by the last author, without knowledge of

the Phase-I results. Hence, it was also a blind test. The performance of this optimum airfoil was then used as a goal to achieve in Phase-III.

The third phase revisits the MDOPT investigations, however, now with insight to the potential improvement possible demonstrated in Phase-II. This one piece of extra knowledge made a significant difference.

Phase-I: Initial MDOPT/OVERFLOW Exercise

As noted above, this phase is a discovery exercise for the first three authors. Here, many complete optimizations were conducted to help advance our knowledge-base up the learning curve for this particular blind-test model problem. The numerous repeats were also necessary to obtain self-consistant results. For example, the optimum drag level obtained in the N-space should be no worse than that achieved in the M-space, where $3 \leq M \leq N$. Initially, to obtain this behavior, or close to it, required much effort. Specifically, the range of the design variables have to be manipulated. If the user-defined range of a DV is too small, or not well centered, then the region of the design space studied may not contain the global optimum. Yet, if the range of the DVs is too large, then the response surface from the design of experiments (DOE) can become so inaccurate that only false optimums are persued. Unfortunately, the pertinent information required to set such ranges is not known *a priori*; it is accumulated with applied experience on a given class of problems.

Within the MDOPT environment, the geometric constraint of Eqn (7) is approximated with 11 evenly-spaced spar constraints. A constraint on the maximum TE included angle is also added. Each constraint is enforced with its own response surface. Under this implementation, it is possible for the exact constraint of Eqn (7) to be violated.

Figure 5 provides a typical convergence history of an MDOPT Response-Surface optimization for the Bez4-0012 airfoil in 12-space. Note that this figure starts with Case-257 and ends with Case-567. The first 256 cases correspond to an initial seeding of the design space. Here, a design of experiments (DOE) distributes these cases based on a Latin hypercube spanning the user-specified region of the design space. This figure depicts the response-surface estimates with corresponding truth values, as well as, tracks the best truth-verified cases with a monotonically-decreasing line. Note that the best design resulting immediately from this 256-case DOE had $C_{Dopt} \sim 318$ counts, while the remainder of this optimization reduced the drag about another 35 counts.

Figure 6 shows a comparison of the convergence histories of best airfoil shapes for [6,12,24,36] design variables. In general, note that as the design-space dimension increases, the number of cases required for convergence increases, while the drag of the optimum geometries improve, at least until the 36-space result.

Table III gives final optimum-drag values obtained in Phase-I as a function of design-space dimension. Note that the baseline Bez4-0012 airfoil corresponds to NDV=0 where its drag is 468.9 counts according to OVERFLOW. For reference, NACA0012 has 469.6 counts of drag at this flow condition, per OVERFLOW.

Table III: Phase-I MDOPT Results.

NDV	No. Cases	C_{Dopt}
0	1	468.9
6	278	327.0
12	567	283.4
24	1,258	243.4
36	2,324	249.3

Figure 7 is a plot of the data from Table III which illustrates how the drag of the optimum geometries improves with design-space dimension. The interesting characteristic of this trend is that the drag of the optimum in 36-space is worse than that found in 24-space. Since all supported geometries in 24-space are fully contained in 36-space, one explanation for this reversal is that the optimization process simply has not yet found the optimum geometry, even after 2,324 cases have been analyzed. This could also be a consequence of the user-specified range on DVs in 36-space inadequately capturing the pertinent geometries of the 24-space run.

The number of coefficients defining a quadratic response surface is: $NCoef = \frac{NDV*(NDV+1)}{2}$. Further, the computational effort required to determine the coefficients for a response surface scales with the number of unknowns cubed. Hence, the build time of the DOE response surfaces is $\mathcal{O}(NDV^6)$. Data collected on this are tabulated in Table IV and illustrated in Figure 8. This figure shows that the asymptotic slope of the

trendline is 6.0, and hence, is consistent with that expected. Note that the data of Table IV does not include the time required to evaluate the objective functions of the DOE, where the number of cases in a DOE must be greater-than or equal-to the number of the unknown coefficients. Hence, $NDOE = \mathcal{O}(NDV^2)$.

Table IV: DOE Response-Surface Build Times.

NDV	$NCoef$	No. DOE Cases	CPU (sec)
6	21	121	7
12	78	256	157
24	300	529	3,341
36	666	1,369	38,042

Phase-II: SYN83 Investigation

In this phase, the last author conducted a SYN83 optimization on the model problem. This effort was performed without knowledge of the MDOPT results of Phase-I, and therefore, was also conducted as a blind test. Since the design space for SYN83 is essentially the highest dimensional space supported by the discrete grid, the performance of the resulting optimum airfoil could provide a limit to what is achievable.

Figure 9 provides a SYN83 solution about the baseline Bez4-0012. The left side of this figure includes the pressure distribution of this symmetric solution, while the right side depicts the Mach contours in the near field about Bez4-0012. Note the strong shock of this case which yields a drag coefficient of 457.0 counts. The discrepancy in drag predictions between SYN83 and OVERFLOW is about 2.5% for the Bez4-0012 baseline airfoil.

Figure 10 provides a SYN83 solution for the optimum airfoil derived by SYN83. This airfoil has been designated BJ5XE. The shock strength of the optimum airfoil is much diminished relative to the baseline. According to SYN83, the drag coefficient for the BJ5XE optimum airfoil is about 104.4 counts, yielding a total reduction of more than 350 counts relative to the baseline Bez4-0012 airfoil. This finding is significantly better than anything discovered in Phase-I.

Phase-III: Final MDOPT/OVERFLOW Study

Due to the large disparity between the results of the first two phases, a third phase was initiated to reopen the MDOPT study of Phase-I. Comparison of the BJ5XE airfoil with optimum geometries of Phase-I uncovered the issue. The TE included angle of BJ5XE was much larger than that of any of the Phase-I optimum airfoils. While the optimum airfoils of Phase-I came close to the TE included-angle constraint, they did not reside on this constraint boundary. As a consequence, it was not obvious at the time that this constraint was an issue. By relaxing the constraint on the TE included angle, as well as implementing other lessons learned, the results of Phase-III now align well with those of Phase-II.

Figure 11 shows a comparison of the convergence histories of the best airfoils for [3,6,12,24,36] design variables in Phase-III. In general, as the design-space dimension increases, the drag of the optimum geometries monotonically improves. Further, the number of cases required to achieve convergence increases with NDV.

Table V tabulates the final optimum-drag values obtained in Phase-III as a function of design-space dimension. Again note that the baseline Bez4-0012 airfoil result corresponds to $NDV = 0$.

Table V: Phase-III MDOPT Results.

NDV	No. Cases	Optimum Case	C_{Dopt}
0	1	-	468.9
3	546	359-1	312.5
6	1,349	1281-1	221.5
12	1,787	1729-1	139.5
24	2,377	2315-1	117.6
36	3,034	3020-1	103.8

Figure 12 is a plot of the data from Table V which illustrates how the drag of the optimum geometries improves with design-space dimension. As can be seen in this figure, drag of the optimum airfoils follow a monotonically decreasing trendline with NDV. Furthermore, this trend is approaching the level established by SYN83 on the BJ5XE optimum airfoil.

Figures 13-17 provide a comparison of the knots of the baseline Bez4-0012 airfoil with those of the best airfoil shapes for [3,6,12,24,36] design variables, respectively. In each of these figures, the baseline Bez4-0012 knots (solid symbol) and optimum-airfoil knots (open symbol) are depicted in the corresponding N-space and the Y coordinate is amplified to ease visual comparison.

Figure 18 provides a comparison of the baseline Bez4-0012 airfoil (solid line, no symbol), with the best airfoil shapes for [3,6,12,24,36] design variables (open symbols), and includes the SYN83 BJ5XE airfoil (solid symbol). The Y coordinate is amplified to enhance visual comparison. It is gratifying to see that the optimum airfoils of Phase-III are approaching BJ5XE as the dimension of the design space increases.

Figure 19 provides a comparison of the pressure distributions of the baseline Bez4-0012 airfoil with those of the optimum shapes for [3,6,12,24,36] design variables. It is interesting to note that the shock strengths of each of these geometries appear to be essentially the same. The pressure level just upstream of the shock is $C_p \sim -0.9$ and jumps to a level of $C_p \sim +0.1$ just downstream of the shock. Yet the drag levels of these airfoils range from about 100 counts to about 470 counts. To understand how this can be, one must inspect the flowfield, not just the properties on the airfoil surface. Refer back to Figures 9-10 which illustrate the flowfield Mach contours for the baseline Bez4-0012 and BJ5XE airfoils, respectively. Note that the shock of the Bez4-0012 airfoil extends about 75% of a chord-length off the surface into the flowfield. Whereas the shock system of the BJ5XE airfoil is comprised of two parts: 1) a strong normal shock adjacent to and extending from the airfoil to about 5% of a chord-length into the flowfield, and 2) a weak curved shock which extends from about 5%-to-75% of a chord-length off the surface into the flowfield.

IX. Conclusions

A model problem of aerodynamic shape optimization has been studied. The objective function for this model problem is relatively inexpensive to evaluate, yet provides an essential element of nonlinear behavior to be challenging. The seed geometry, designated Bez4-0012, is an optimal approximation of the NACA0012 airfoil, as defined by a 4^{th}-order Bezier curve. In order to systematically study the impact of dimensionality, an infinite family of design spaces was developed. This family has the property that all airfoil shapes supported in its M-space are fully and exactly contained within its N-space, where $3 \leq M \leq N$. Two approaches to optimization were studied. The MDOPT environment exercised a response-surface approach, while SYN83 utilized a gradient-based technique.

The present study was partitioned into three chronological phases. The first phase provided time for discovery, the second phase provided an independent optimization to the model problem, and the third phase augmented information from the first two phases, yielding much-improved results. Results for design-space dimensions of $[3, 6, 12, 24, 36]$ are presented. These data include trends with respect to increasing dimension on realized minimum-drag designs, and computational costs.

The data show that as the dimension of the design-space increases, the optimum design monotonically improves, and appears to asymptotically approach a limiting value. The SYN83 optimum design (BJ5XE) is consistent with this limiting value. For the response-surface approach, the computational costs required to identify the optimum increases with number of design variables. Here, the number of cases required scale with $\mathcal{O}(NDV)$, however, the cost of building the DOE response surfaces scales with $\mathcal{O}(NDV^6)$.

X. Post Script

Conducting basic research can often yield unexpected results. After Phase-II was completed, the bookend authors wondered, "At what Mach number would the model problem yield an optimum airfoil with zero shock drag?" To help scope an answer to this question, the BJ5XE airfoil was analyzed at slightly reduced freestream Mach numbers. What we found surprised us; the zero-lift condition for this symmetric airfoil at $\alpha = 0^\circ$ became unstable for $M \sim 0.845$. The model problem turned pathological. This finding spawned a follow-on study in search of simple symmetric airfoil shapes that support non-unique inviscid compressible flow solutions at 0° angle-of-attack. Please see Jameson, Vassberg and Ou.[8]

References

[1]J. C. Vassberg and A. Jameson. In pursuit of grid convergence, Part I: Two-dimensional Euler solutions. *AIAA paper 2009-4114*, 27^{th} AIAA Applied Aerodynamics Conference, San Antonio, TX, June 2009.

[2]I. H. Abbott and A. E. von Doenhoff. *Theory of Wing Sections*. Dover, New York, 1959. ISBN 0-486-60586-8.

[3]R. H. Nichols and P. G. Buning. OVERFLOW User's Manual, Version 2.1t. Technical report, U. of Alabama and NASA, August 2008.

[4]A. Jameson. Solution of the Euler equations for two dimensional transonic flow by a multigrid method. *Applied Mathematics and Computation*, 13:327–356, 1983.

[5]A. Jameson. Artificial diffusion, upwind biasing, limiters and their effect on accuracy and multigrid convergence in transonic and hypersonic flows. *AIAA paper 93-3359*, AIAA 11th Computational Fluid Dynamics Conference, Orlando, Florida, July 1993.

[6]S. T. LeDoux, W. W. Herling, G. J. Fatta, and R. R. Ratcliff. MDOPT - A multidisciplinary design optimization system using higher-order analysis codes. *AIAA paper 2004-4567*, 10^{th} AIAA/ISSMO Multidisciplinary Analysis and Optimization Conference, Albany, NY, August 2004.

[7]A. Jameson. Efficient aerodynamic shape optimization. *AIAA paper 2004-4369*, 10^{th} AIAA/ISSMO Multidisciplinary Analysis and Optimization Conference, Albany, NY, August 2004.

[8]A. Jameson, J. C. Vassberg, and K. Ou. Further studies of airfoils supporting non-unique solutions in transonic flow. *AIAA paper 2011-0000*, 20^{th} AIAA Computational Fluid Dynamics Conference, Honolulu, HI, June 2011.

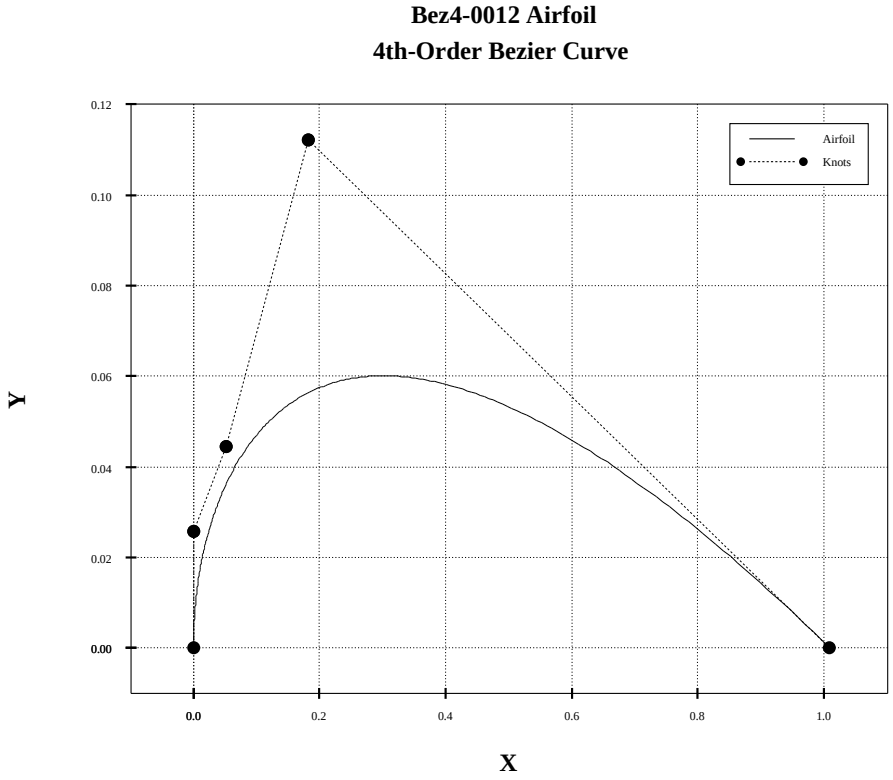

Figure 1. Bez4-0012 Airfoil and 4^{th}-Order Bezier Knots.

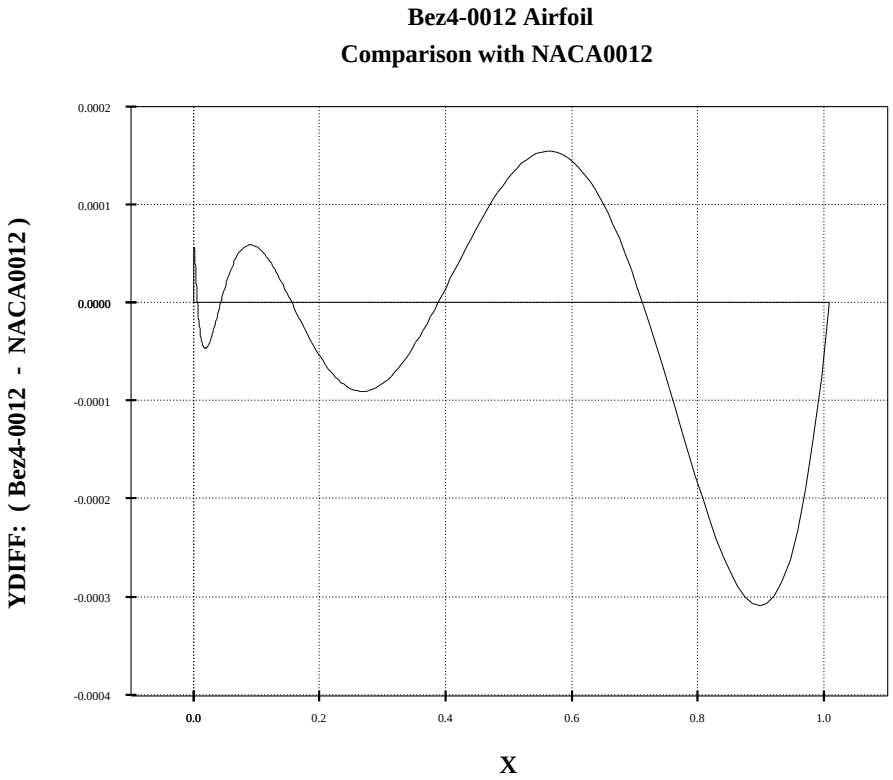

Figure 2. Difference Between Bez4-0012 and NACA0012 Airfoils.

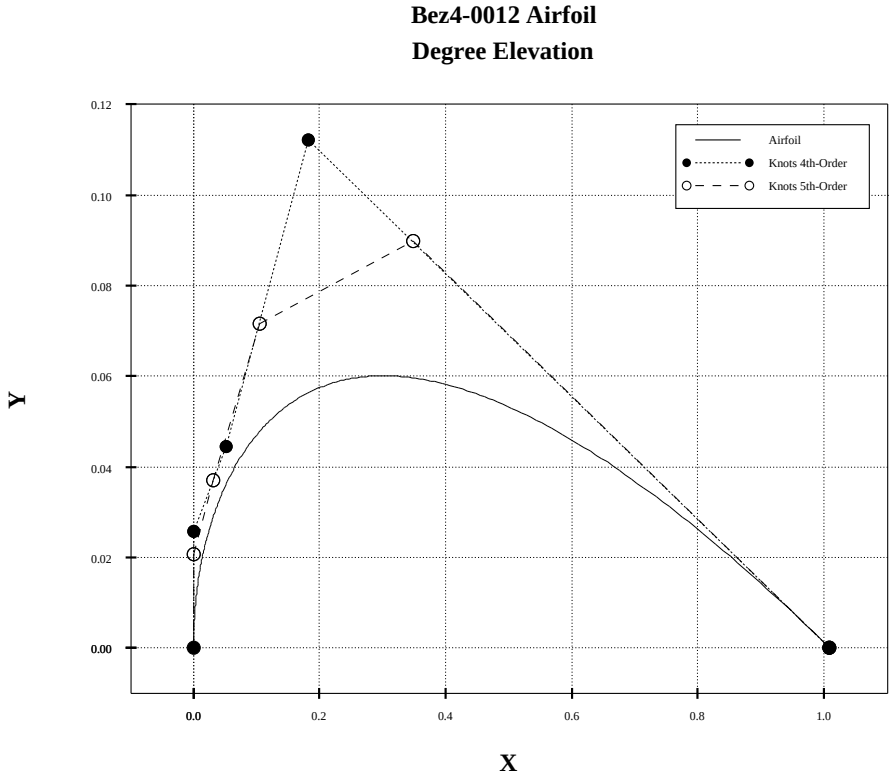

Figure 3. Degree Elevation of Bez4-0012 Curve from 4^{th} to 5^{th} Order.

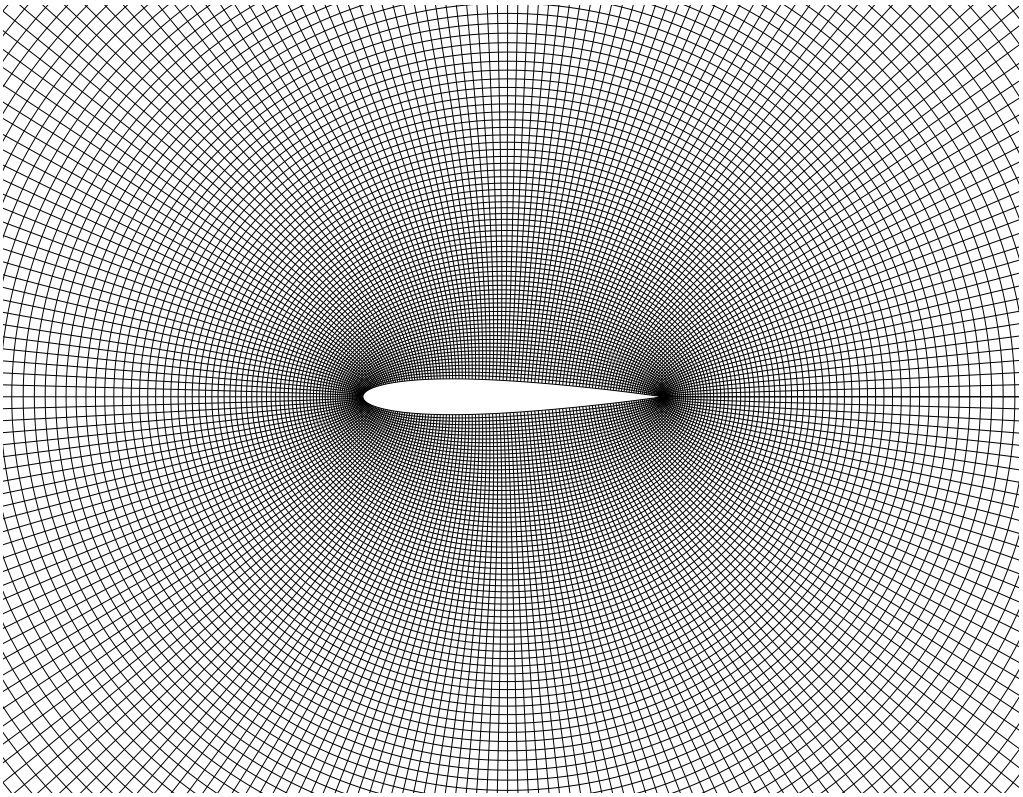

Figure 4. Close-up view of the NACA0012 256x256 O-mesh.

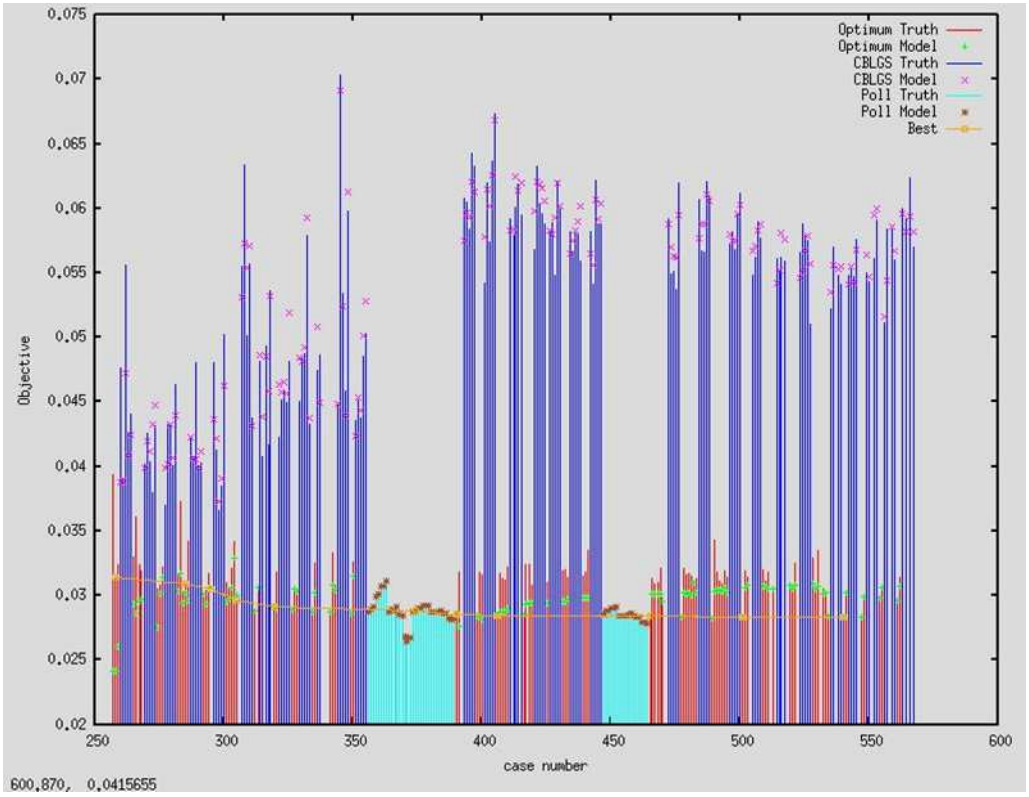

Figure 5. Typical Drag Reduction History of MDOPT Response Surface for 12 Design Variables.

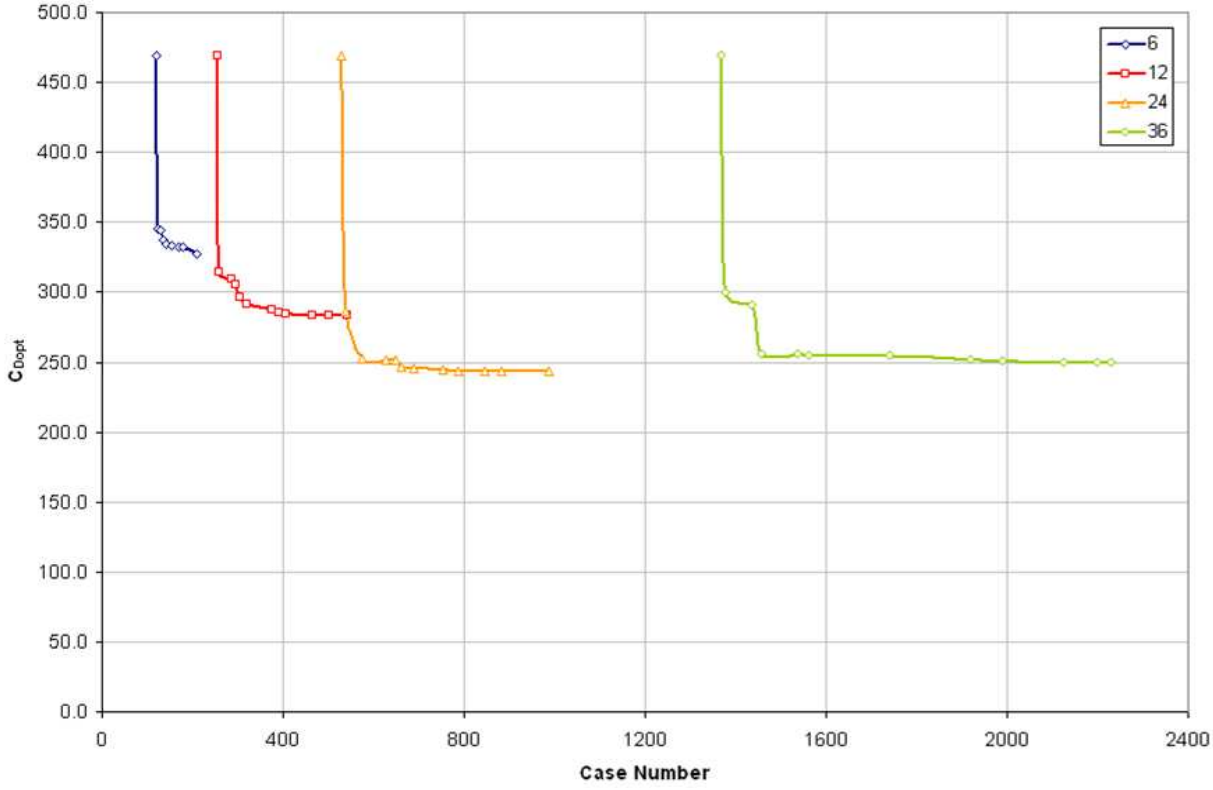

Figure 6. MDOPT Drag Reduction Histories for Various Design Spaces in Phase-I.

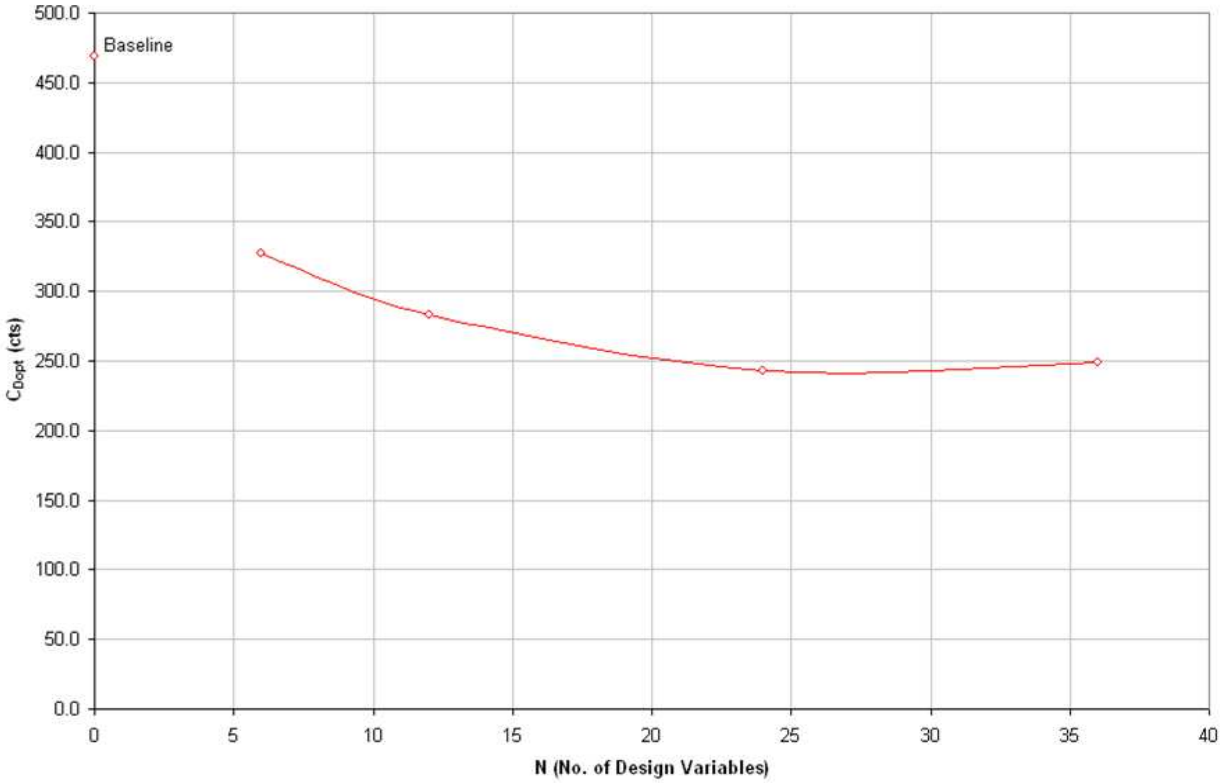

Figure 7. Optimum Realized Drags for Design Spaces of $NDV = [0, 6, 12, 36]$ in Phase-I.

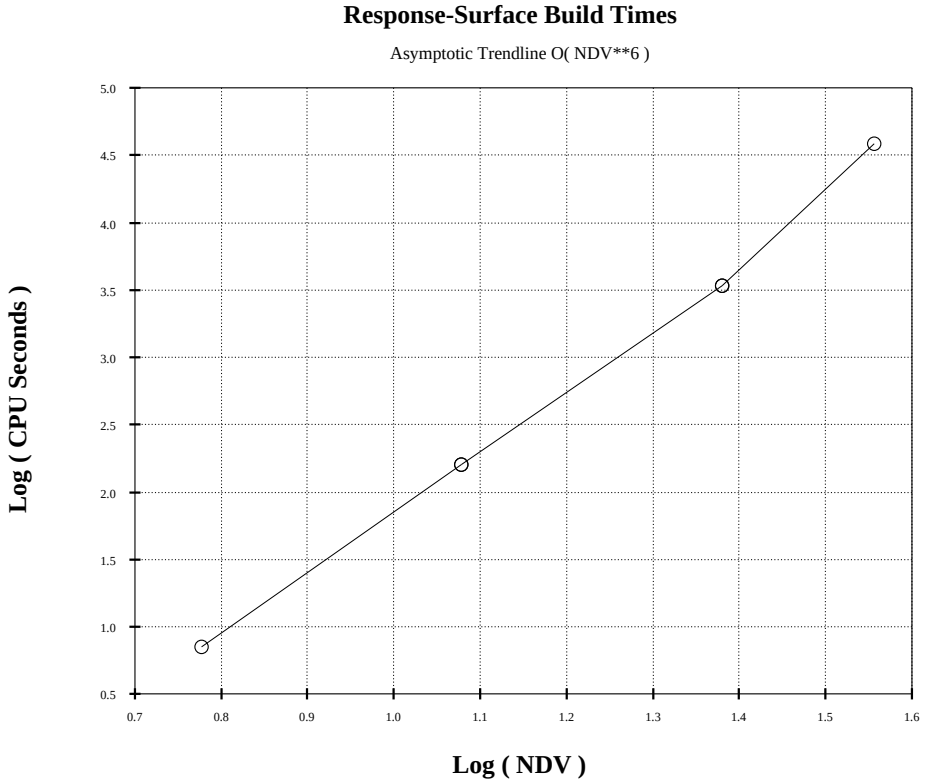

Figure 8. MDOPT Response-Surface Build-Time Trendline.

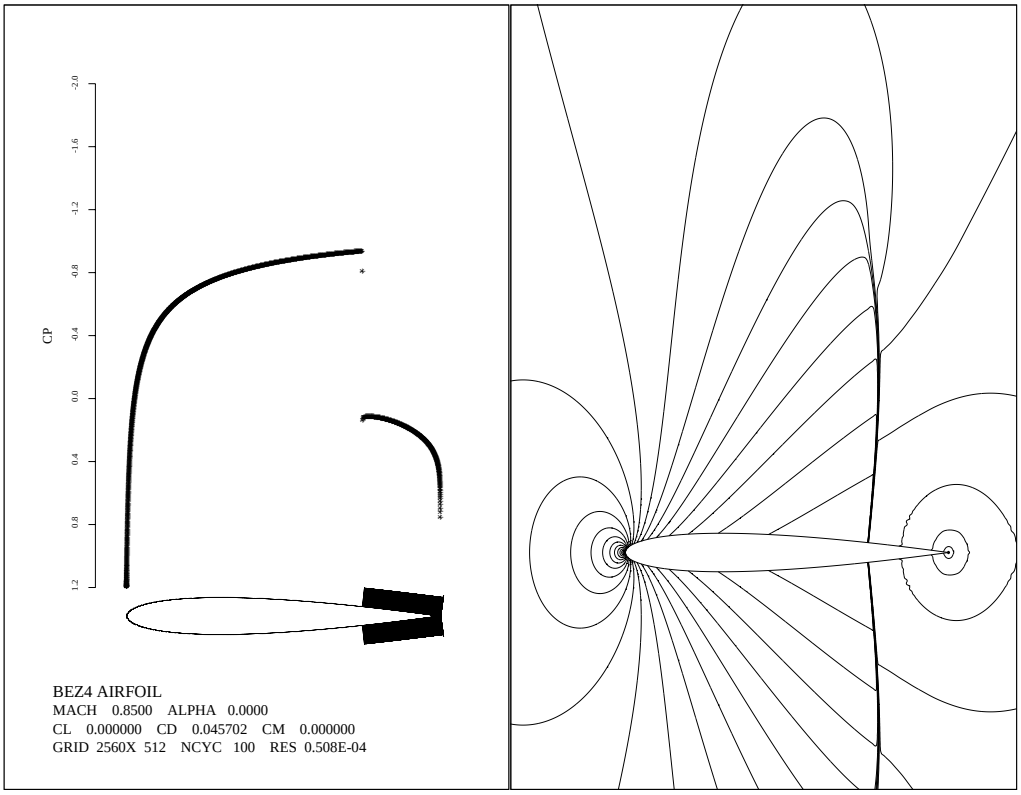

Figure 9. SYN83 Solution on the Bez4-0012 Baseline Airfoil.

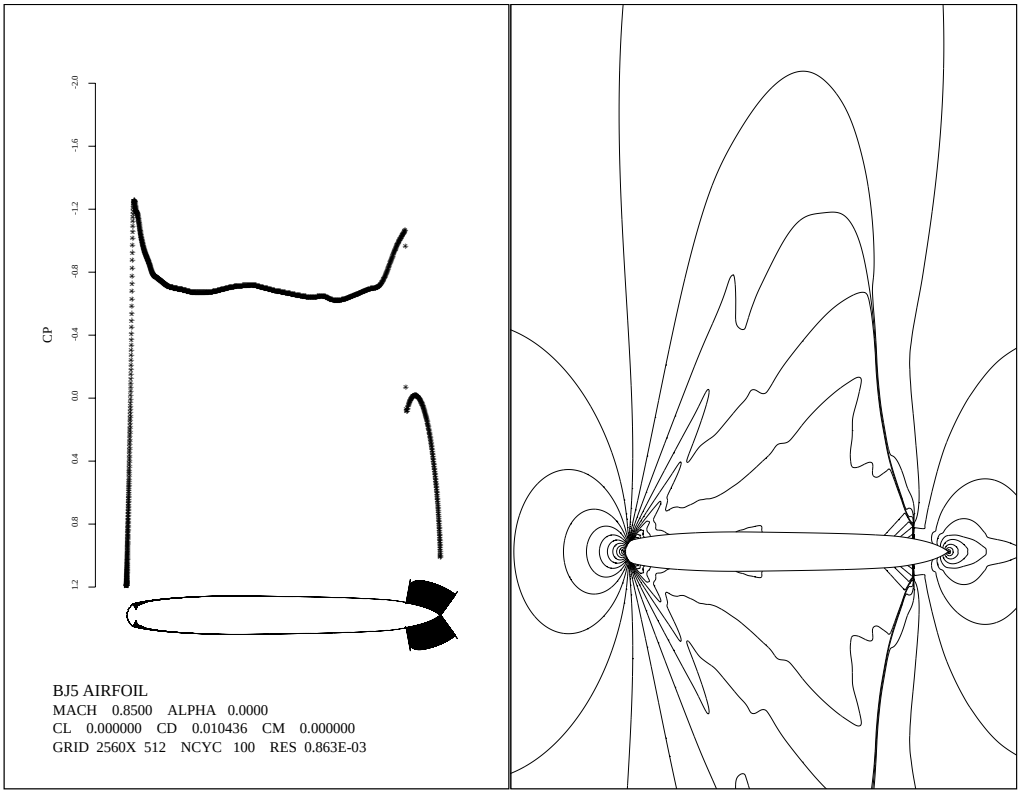

Figure 10. SYN83 Solution on its Optimized BJ5XE Airfoil.

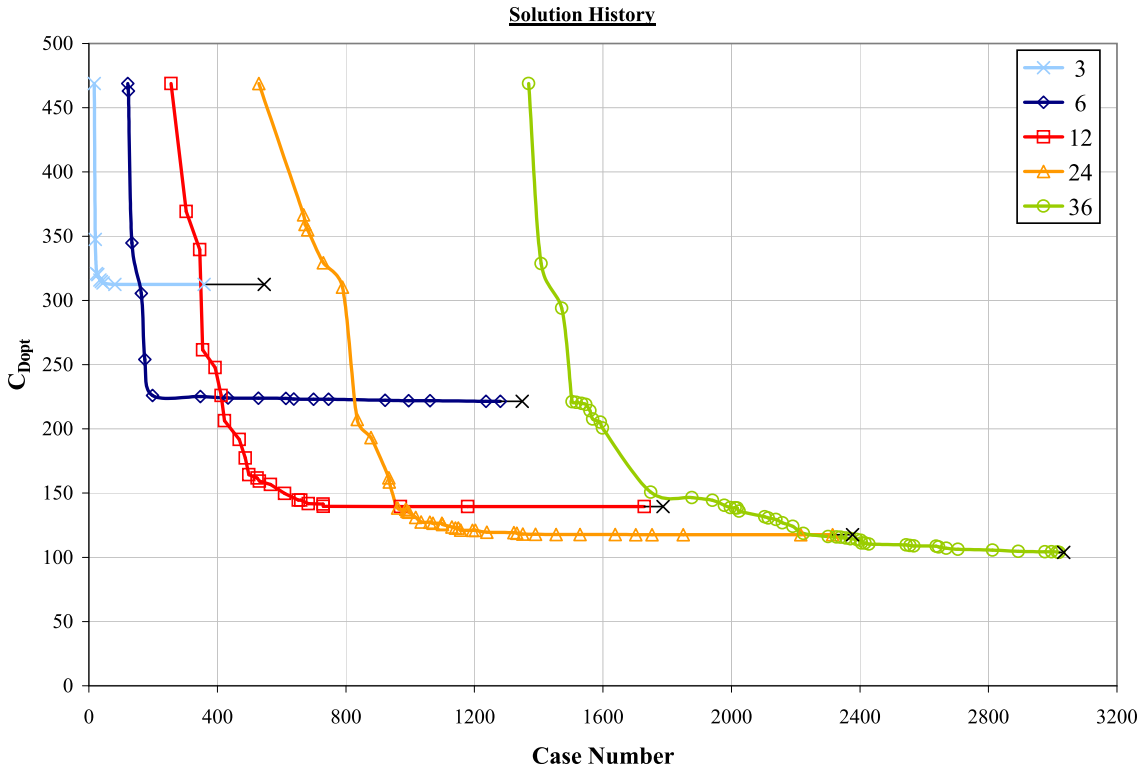

Figure 11. MDOPT Drag Reduction Histories for Various Design Spaces in Phase-III.

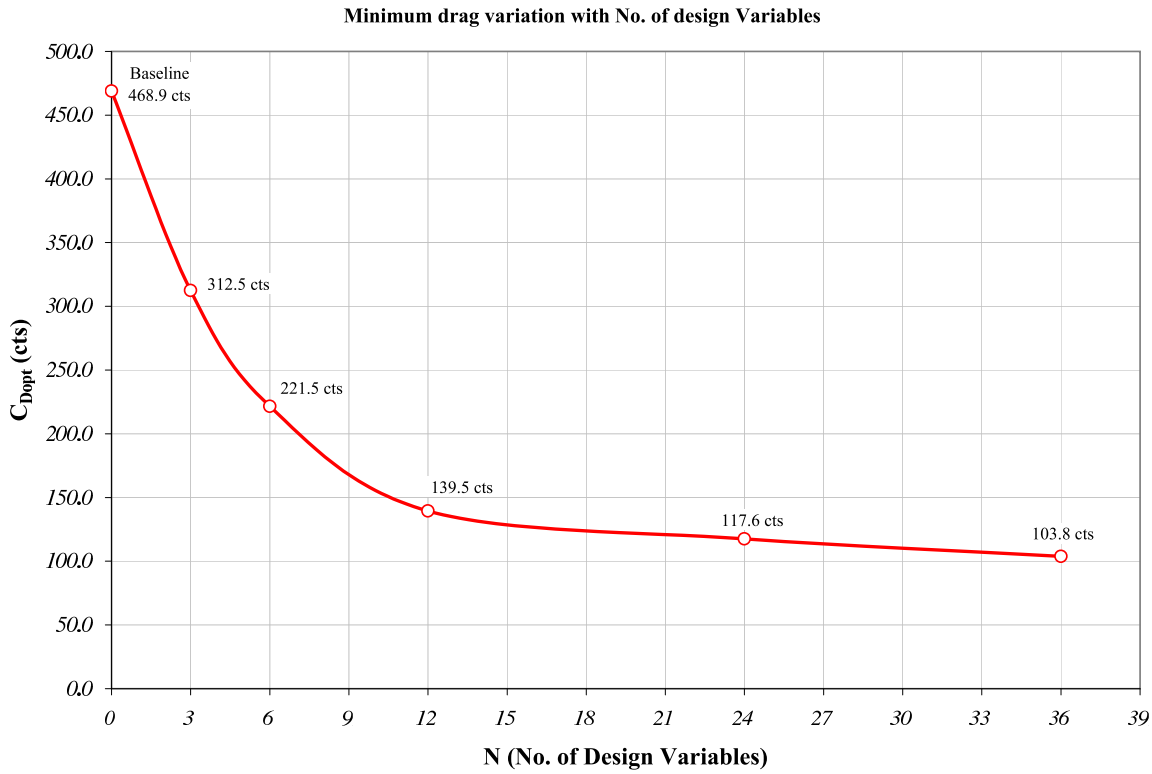

Figure 12. Optimum Realized Drags for Design Spaces of $NDV = [0, 3, 6, 12, 24, 36]$ in Phase-III.

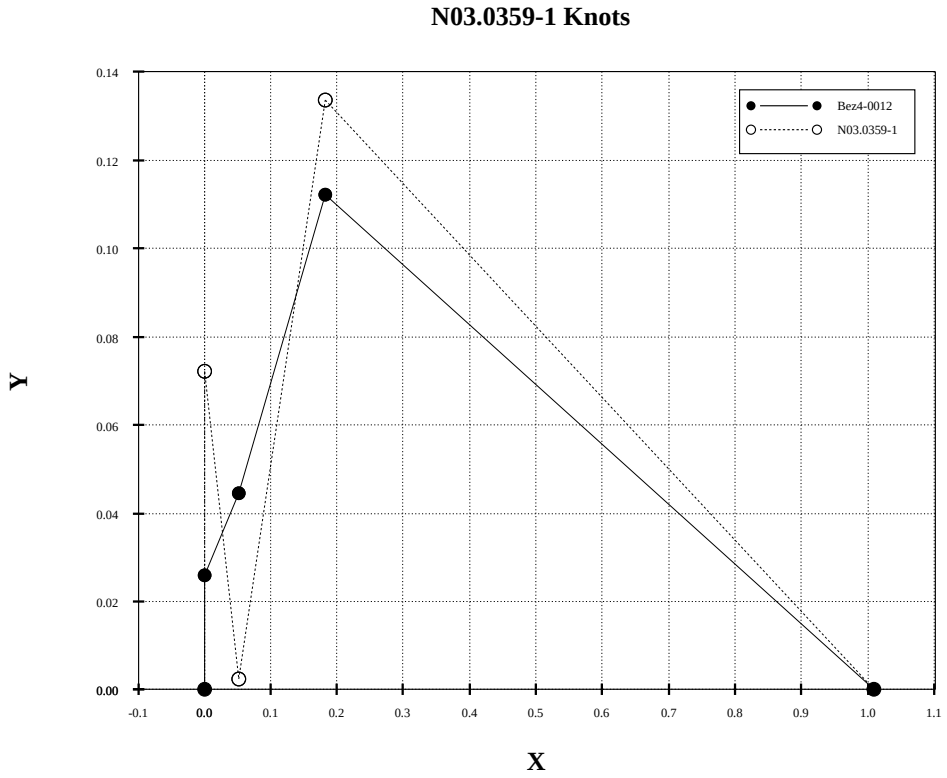

Figure 13. Comparison of Bez4-0012 and MDOPT Optimum Knots for $NDV = 3$.

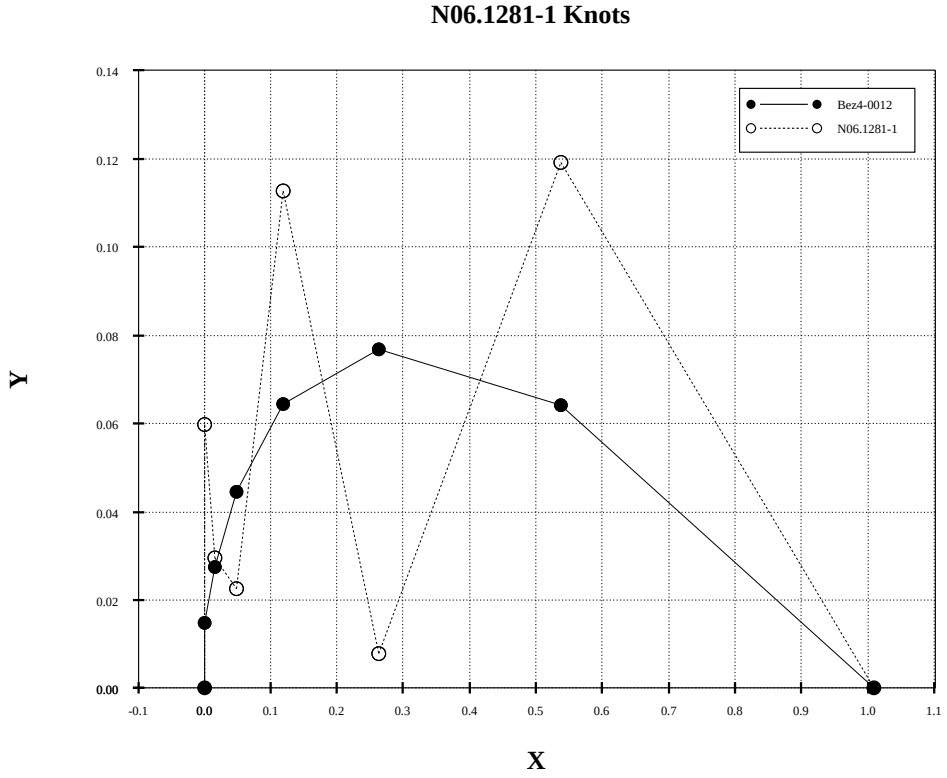

Figure 14. Comparison of Bez4-0012 and MDOPT Optimum Knots for $NDV = 6$.

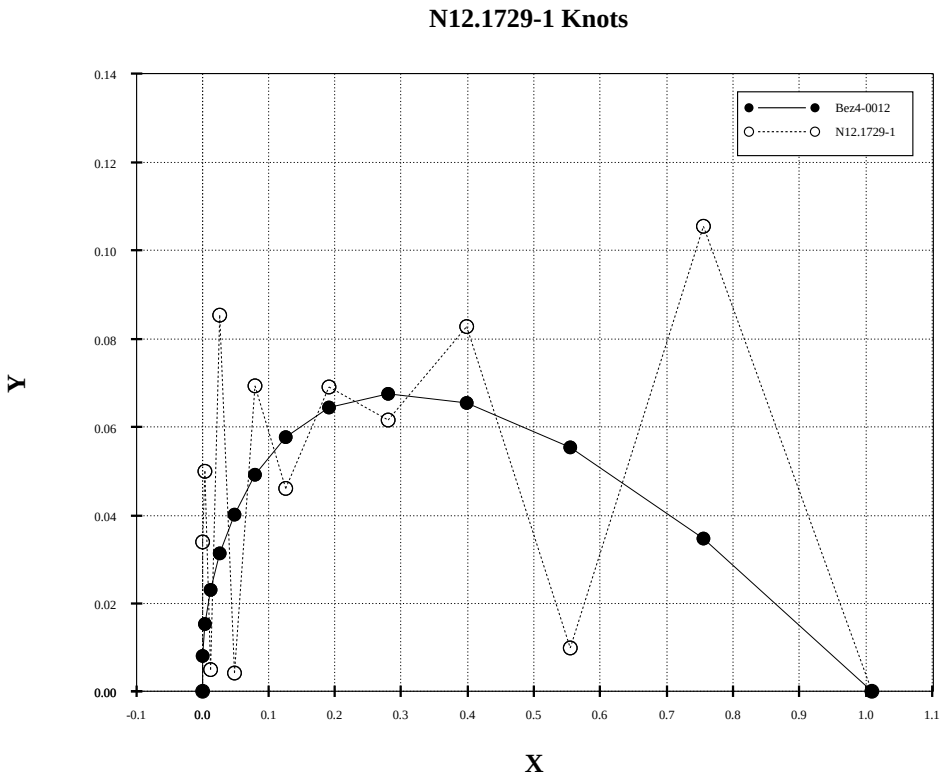

Figure 15. Comparison of Bez4-0012 and MDOPT Optimum Knots for $NDV = 12$.

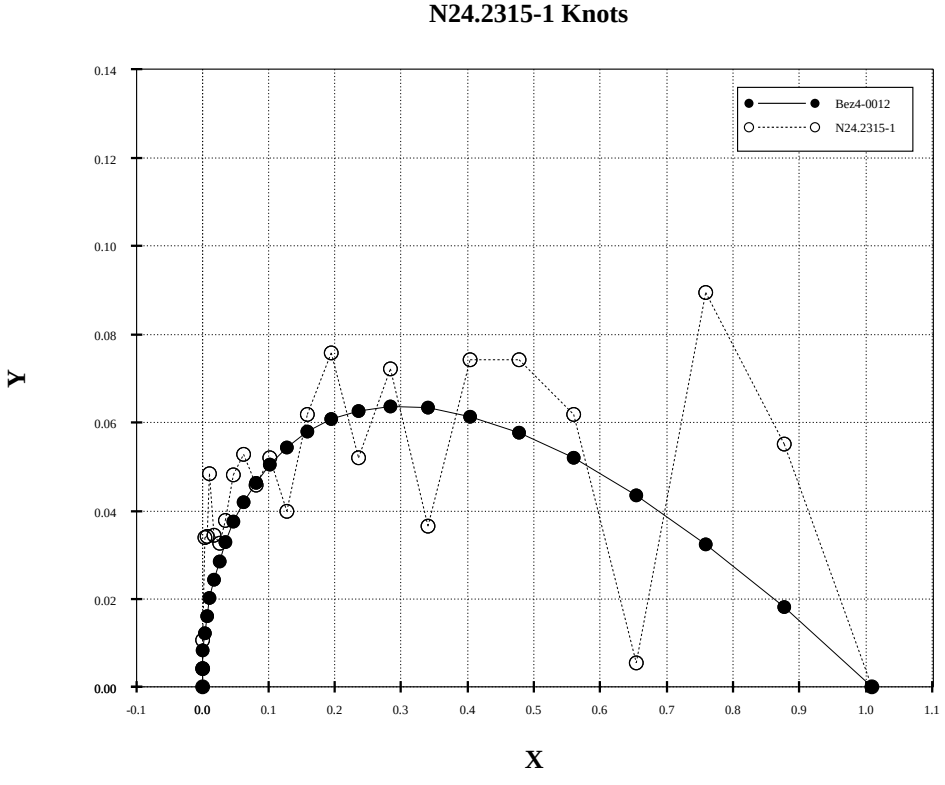

Figure 16. Comparison of Bez4-0012 and MDOPT Optimum Knots for $NDV = 24$.

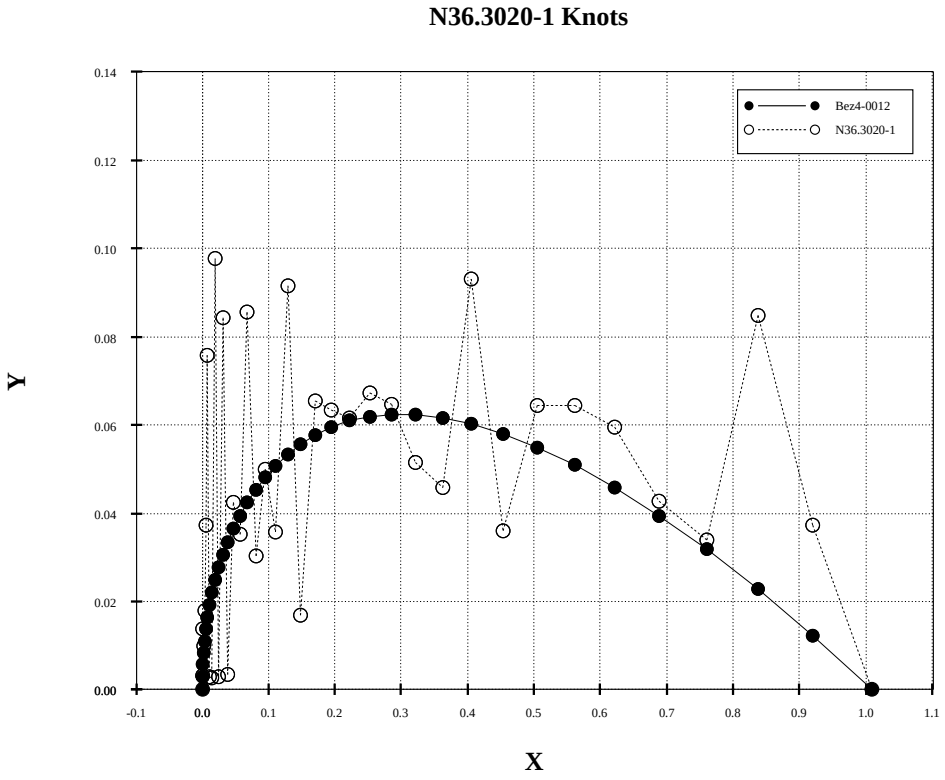

Figure 17. Comparison of Bez4-0012 and MDOPT Optimum Knots for $NDV = 36$.

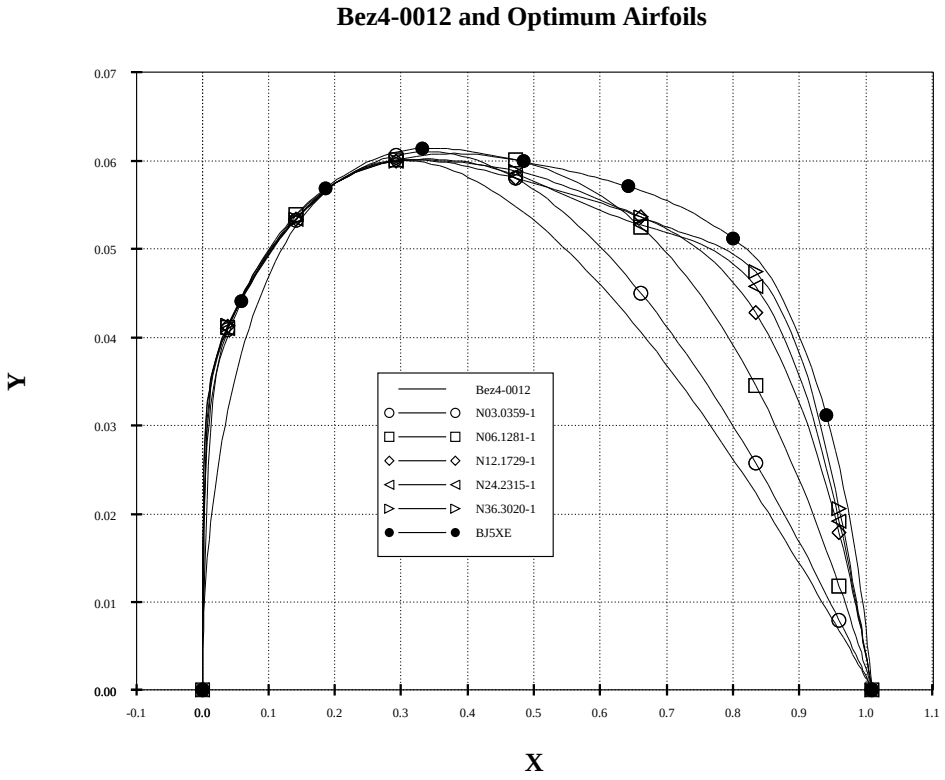

Figure 18. Comparison of Bez4-0012, MDOPT Optimums and BJ5XE Airfoils.

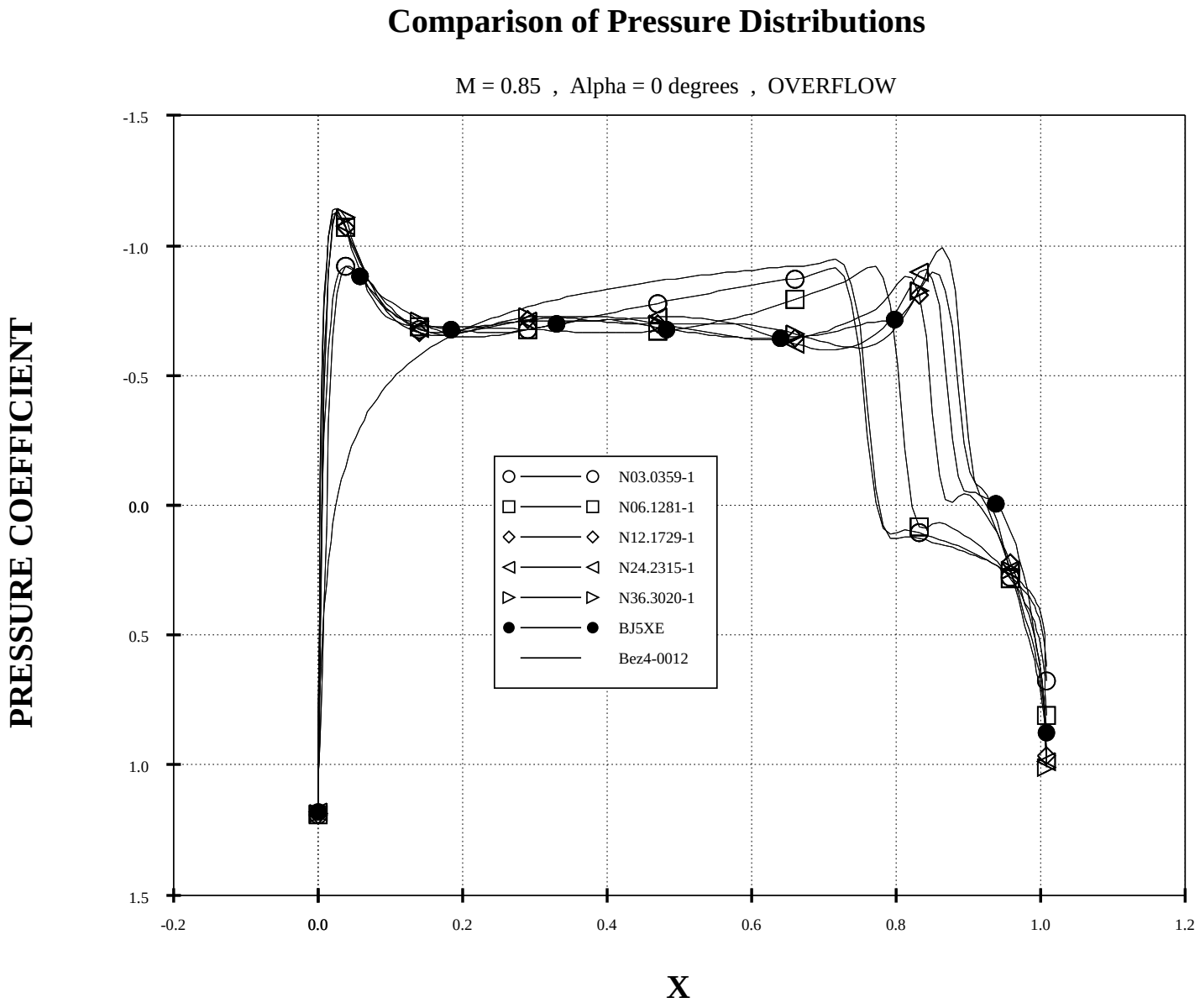

Figure 19. Comparison of Pressure Distributions for Bez4-0012, MDOPT Optimums and BJ5XE Airfoils.